PROCEEDINGS OF SPIE

SPIEDigitalLibrary.org/conference-proceedings-of-spie

Low coherence interferometry to characterize the induced vibrations and topology change of the cryogenic mirror of the Einstein Telescope prototype

Jesús Vilaboa Pérez, Marc Georges, Cédric Lenaerts, Jérôme Loicq

Jesús Vilaboa Pérez, Marc Georges, Cédric Lenaerts, Jérôme Loicq, "Low coherence interferometry to characterize the induced vibrations and topology change of the cryogenic mirror of the Einstein Telescope prototype," Proc. SPIE 12188, Advances in Optical and Mechanical Technologies for Telescopes and Instrumentation V, 121881E (29 August 2022); doi: 10.1117/12.2629402

Event: SPIE Astronomical Telescopes + Instrumentation, 2022, Montréal, Québec, Canada

SPIE.

Downloaded From: https://www.spiedigitallibrary.org/conference-proceedings-of-spie on 20 Dec 2022 Terms of Use: https://www.spiedigitallibrary.org/terms-of-use

Low coherence interferometry to characterize the induced vibrations and topology change of the cryogenic mirror of the Einstein Telescope prototype

Jesús Vilaboa Pérez[a], Marc Georges[a], Cédric Lenaerts[a], and Jérôme Loicq[a,b]

[a]Centre Spatial de Liège (CSL), STAR Institute, Université de Liège, Avenue du Pré-Aily, 4031, Liège, Belgium

[b]Faculty of Aerospace Engineering, Delft University of Technology, Delft, 2629 HS, Netherlands

ABSTRACT

We describe the state of development of a white light interferometer to characterize the cryogenic mirrors for GW detector on operation. We include the first experimental results from the proof of concept of the metrology instrument. The instrument will characterize the topology as well as the vibration of the mirrors. This development takes place in the frame of the E-TEST project. E-TEST is one of the technology demonstrators for the future Einstein Telescope (ET). ET is dedicated to the measure and characterization of gravitational waves. The prototype built by E-TEST includes a large silicon mirror of 40 cm diameter suspended by innovative vibration isolation hanging modules. To reach the detection specification, the mirror is cooled down at cryogenic temperatures around 20 K. Nevertheless, even after the isolation, the mirror may not reach perfect stability once at cryogenic temperatures. Furthermore, the mirror may experience surface topology changes and wavefront deformation due to the extreme variations in temperature and gradient. With our metrology instrument, we can obtain on a single camera frame a set of interferogram maps of the area observed on the mirror at different optical path differences. To do this, we design an innovative phase mask for a white light low-coherence interferometer. In addition, we implement new algorithms for the white light interferogram analysis, avoiding the limitations of the conventional Phase Shifting Interferometry algorithms.

Keywords: White Light Interferometry, Dynamical Interferometry, Optical Phase Mask, Single-Frame low-coherence Interferometry, Topology and vibration determination with interferometry

1. INTRODUCTION

The gravitational waves have a significant impact on the scientific community. These ripples in space-time generated by the highest energetic processes in the universe contain the key to explaining some of the largest physical phenomena. The Einstein Telescope is a third-generation gravitational waves detector. The Einstein Telescope EMR Site Technology (E-TEST) project aims to realize a cryogenic damping prototype for the Einstein Telescope. E-TEST includes a silicon mirror of 40 cm diameter, suspended and cooled down at cryogenic temperatures around 20 K.[1] During the cooling down, the mirror may be affected by surface topology changes and induced vibrations. H. Kaneda et al. proved the topology change of a large mirror at cryogenic temperatures.[2] In the framework of the Einstein Telescope, the mirror characterization is essential to ensure the accuracy of the results in the detection of gravitational waves.

We update on the state of development of a dynamic or single-frame white light interferometer to characterize the cryogenic mirrors for a Gravitational Wave detector on operation.[3] The metrology instrument measures the local vibration as well as the topology change of the suspended silicon mirror at cryogenic temperatures. We also present the advancements in the optical simulations and the development of a proof of concept of the instrument at the laboratory. The objective of the proof of concept is to study the instrument's feasibility and prove the results obtained from the simulations through a concept version of the instrument. We illustrate the

Further author information: (Send correspondence to J.V.P.)
J.V.P.: E-mail: jvilaboaperez@uliege.be

Advances in Optical and Mechanical Technologies for Telescopes and Instrumentation V, edited by Ramón Navarro, Roland Geyl, Proc. of SPIE Vol. 12188, 121881E
© 2022 SPIE
· 0277-786X · doi: 10.1117/12.2629402

Downloaded From: https://www.spiedigitallibrary.org/conference-proceedings-of-spie on 20 Dec 2022
Terms of Use: https://www.spiedigitallibrary.org/terms-of-use

interferograms obtained with a source with a bandwidth at its Full Wave Half Maximum (FWHM) of around 400 nm on the visible spectral range between 400 nm to 800 nm. Therefore the source coherence length is very low. We comment on the limits we found and propose solutions to improve the contrast and definition of the interferograms.

With our interferometer, we obtain at each camera frame a set of interferogram maps of the area observed on the mirror at different Optical Path Differences (OPD). We do not use PZT devices to avoid unwanted additional vibrations. The added value of the interferometer is the possibility of monitoring the vibration and topology change of multiple local areas on the mirror and not just a single absolute value. To make this possible we designed an innovative phase mask working on transmission. The phase mask has a stair shape made of steps of different optical thicknesses of the same material. We will discuss how the phase mask design depends on multiple parameters such as the coherence length of the source, the size of the minimum detail we want to observe or the algorithm to process the white light interferograms.

We use a low-coherence source to unambiguously determine the mirror location and therefore the local vibration and topology. The interference pattern of a low-coherent white light source is characterized by a well-differentiated central fringe visible only close to the optical contact[4].[5] The difficulty in obtaining the interference fringes with a low-coherence source is an advantage to avoiding spurious unwanted interferometry signals from scattered rays, speckle, dust, and imperfections.[6] Each step of the phase mask we design will capture a point of the interference pattern. Then we reconstruct the full interference pattern. We do this at multiple local points of the mirror surface. References[7,8,9] explain other techniques to reconstruct an interference pattern on a single camera frame. In Section 2.4 we introduce the new approaches we develop to study the measured interference patterns. We develop new functions since we found some limitations in using traditional processing methods[4,10,11] with our phase mask.

2. METHODS

2.1 Definition of the white light interference pattern

If we assume that the white light source has a Gaussian power spectrum, the interference pattern can be defined as the combination of the normal probability density function and the fundamental equation of interferometry,[12,13,14] obtaining Eq. 1.

$$I(OPD) = 0.5 \cdot I_0 \cdot \left(1 + \exp\left[-\left(\frac{OPD}{lc}\right)^2\right]\right) \cdot \cos\left(2 \cdot k_0 \cdot OPD\right) \tag{1}$$

Where k_0 is the angular wavenumber: $k_0 = 2\ \pi/\lambda$, with λ the central wavelength of the source; while lc is the coherence length defined in Eq. 2.[6] The coherence length defines the distance the wave travels before the temporal coherence drops to zero. As a result, the peak of the white light interference pattern is only visible if the OPD between the two arms of the interferometer is less than half the coherence length of the source. The white light pattern has a periodic modulation with a period of $\lambda/2$.

$$lc = \sqrt{\frac{2\ln(2)}{\pi n}} \frac{\lambda_0^2}{FWHM(\lambda)} \tag{2}$$

We defined the Full Wave Half Maximum (FWHM) at the 1/e of the highest point of the coherence envelope of the interference pattern, obtained by the exponential function in Eq. 3. While n is the index of refraction of the medium where the light propagates and λ_0 in the central wavelength of the source.

$$\text{Coherent envelope} = \exp\left[-\left(\frac{OPD}{lc}\right)^2\right] \tag{3}$$

With the previous equations, we can define a perfect white light pattern like in Fig. 1.

Downloaded From: https://www.spiedigitallibrary.org/conference-proceedings-of-spie on 20 Dec 2022
Terms of Use: https://www.spiedigitallibrary.org/terms-of-use

2.2 Measurement of local vibrations

The initial position of the suspended silicon mirror is unknown due to its non-perfect stability. To compute the local vibration, we use the pair of interferograms measured in two consecutive camera frames. First, we precisely determine the peak of the coherence envelope of each pattern with one of the procedures described in section 2.4. Then, we compute the local vibration between two frames as the distance between the two peaks identified. This distance should be zero in an ideal case where the mirror is perfectly isolated from vibrations. We illustrate the procedure in Fig. 1. In this figure, we normalize the intensity to a value between -1 to 1, but the intensity values are always positive. Finally, we apply the method to the consecutive pair of camera frames for each of the points inside the area observed. The measurement of local vibrations is one of the most significant advantages of the instrument we propose.

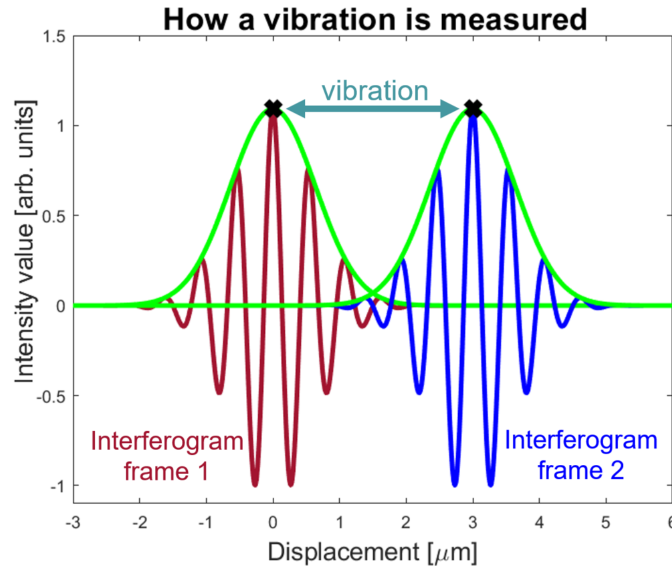

Figure 1. Displacement of the interference pattern between two consecutive camera frames due to vibration.

The second application of the instrument is the measurement of local changes in the topology of the mirror caused by the extreme variation in temperature. At each camera frame, we obtain a set of interferograms that contains the information on the topology of the mirror. Each step of the phase mask corresponds to a region of equivalent size on the detector. We need several camera frames to distinguish a local topology change from a local vibration. We expect the mirror deformation scale to be lower than the vibration scale.

2.3 Working principle of the phase mask

The metrology instrument incorporates an innovative phase mask to perform dynamic white light interferometry. That means having on a single camera frame all the information needed to reconstruct the interference pattern of a local measurement point. In principle, the objective is to capture at the detector a set of interferograms of the same mirror area at different OPDs and on a single camera frame. The phase mask is within an optical layout that ensures that the entire FOV passes by all the phase mask steps. For a specific local point, each step of the phase mask captures a sample point of the white light interference pattern. Then, with all the sample points, we can reconstruct the full white light interferogram. We do this reconstruction of the pattern with all the local points inside the area observed.

The phase mask we conceive has a step design, where each step simulates the change in OPD introduced by the displacement of a PZT device. Each step is made of the same material but has a different optical thickness. If we consider two monochromatic light rays, Eq. 4 gives the OPD between the rays when one traverses a material with an optical thickness e, and the other displaces parallel on air. n is the material index of refraction for a specific wavelength.

Downloaded From: https://www.spiedigitallibrary.org/conference-proceedings-of-spie on 20 Dec 2022
Terms of Use: https://www.spiedigitallibrary.org/terms-of-use

$$OPD = e \cdot (n-1) \tag{4}$$

According to Eq. 4, the change in optical path difference depends on the source wavelength. In our case, we use a polychromatic source. Therefore, the phase shift introduced by a step of the phase mask differs for the individual spectral constituents. This issue is also present in phase-shifting white light interferometers, where a phase shift is introduced by modifying the path length of one of the arms of the interferometer. This issue produces chromatic aberrations that are visible by a shift of the position of the envelope of the white light interference pattern. The shift introduces an error in the measurement of the exact position of the mirror. In addition, these errors appear even if the optical system is well compensated to reduce the chromatic aberration. Nevertheless, the chromatic aberrations related to a phase shift lead to systematic errors in the measurement of the position of the mirror that we can numerically correct.[15]

Figure 2 contains a schematic representation of the mask working principle. We define the height difference between consecutive steps according to the following equation, Eq. 5. We obtain this equation through Eq. 4 to have a representative phase shift of $\pi/2$ between steps.

$$\text{height}_{\text{ difference}} = \frac{\lambda}{8 \cdot (n-1)} \tag{5}$$

In the previous equation, λ is the peak wavelength of the source and n is the material index of refraction for a wavelength. For example, for an index of refraction of around 1.52, which corresponds to N-BK7 with a central wavelength at 500 nm, the height difference between consecutive steps is 120 nm. We expect a surface roughness of the planar region of each step lower than $\lambda/20$ for $\lambda = 633$ nm.

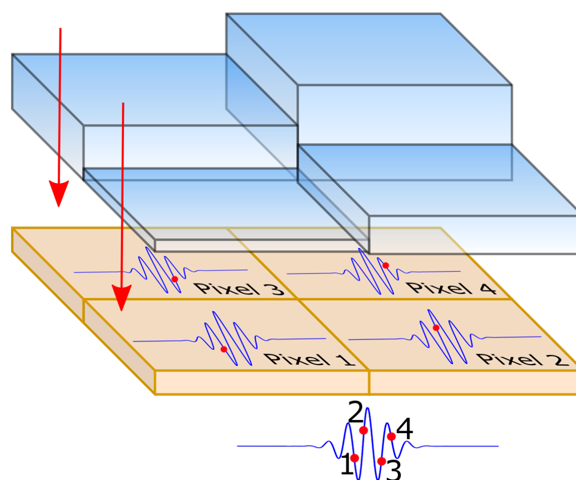

Figure 2. Concept view of the phase mask designed to perform single-frame white light interferometry. Each step captures a sample of the white light interferogram. Then, we can reconstruct the full pattern.

2.4 Determination of the peak of the coherence envelope

The feasibility of the phase mask manufacturing is a critical element for us. The number of steps of the phase mask is based on the sampling of the white light interferogram along the optical axis. As a result, we look for the analysis method that requires the lowest number of samples to reconstruct the white light pattern. We need a reconstruction that allows us to detect the peak of the coherence envelope with the desired accuracy. The detection of this peak is directly related to the mirror position and, therefore, the local vibration and topology change.

First, we discard the analysis methods that require a large set of points to estimate the position of the zero-order fringe. This is the case of the centroid method based on the determination of the centre of gravity

Downloaded From: https://www.spiedigitallibrary.org/conference-proceedings-of-spie on 20 Dec 2022
Terms of Use: https://www.spiedigitallibrary.org/terms-of-use

of the interference pattern.[10] Then, again a large number of data points and big computation times are the reasons to not considered for the moment the frequency-domain analysis methods.[4] In the latter technique, the interference data is transformed into the frequency domain by Fourier analysis and then the relative surface height is determined by calculation of the rate of change of the interferometric phase with the wavenumber.[5] Moreover, to simplify the optical layout and avoid intensity losses through the polarizers, we also discard the possibility of doing a phase shift by a change in the polarization state of the light beam.[16] Our next step was to implement the Phase Shifting Interferometry (PSI) method commonly used in long coherence interferometry. The PSI method computes the relative path difference between the interferometer arms with the interference beam phase. We obtain the phase value with the so-called PSI algorithms, like the one presented in Eq. 6.[17] The PSI algorithms use the intensity of the interference beam measured at different positions of a PZT device. The displacement of the PZT between two sample points must create a phase shift defined by the PSI algorithm. Equation 6 requires a phase shift of $\lambda/8$ or $\pi/4$ between measurements. Several references define different algorithms with more or fewer points, each one with a specific phase shift.[10]

$$\phi = \tan^{-1}\left[\frac{2\left(I_2 - I_4\right)}{2I_3 - I_5 - I_1}\right] \tag{6}$$

Despite the effectiveness of this method, we were not able to obtain acceptable results. This is because we use a phase mask that introduces a phase shift by steps of different thicknesses and a polychromatic source. The phase shift depends on the material index of refraction that depends on the wavelength. As a result, we need flexible and compatible methods with the phase mask we develop if we want to achieve a sub-nanometer resolution. One of the methods we use determines the peak of the coherence envelope by a Hilbert transform. Then, we also define a function based on the product of a cosine and a Gaussian function to fit the intensity points. We illustrate this last method in Fig. 3. In this figure, we normalize the intensity again from -1 to 1, knowing that the intensity value is always positive. The aim is to develop a method for having the best accuracy. This is a mathematical function or analysis method that allows for correctly reconstructing the interferogram even with a faulty sample, unwanted signal noise or uneven phase shifts between samples.

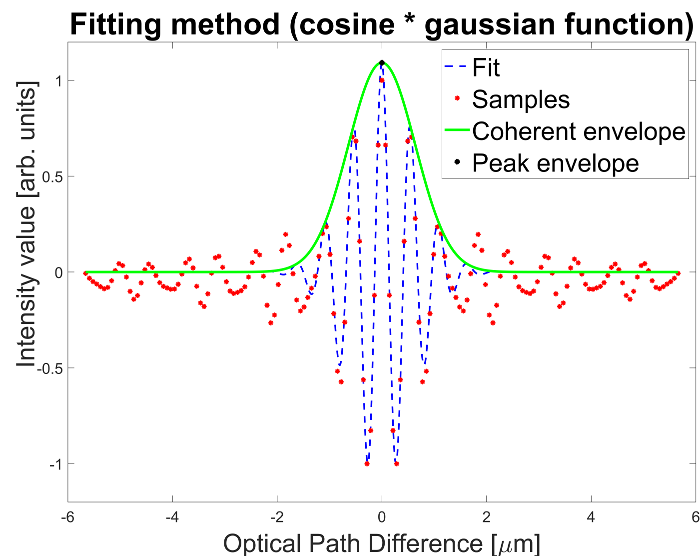

Figure 3. Determination of the peak of the coherence envelope by fitting a mathematical function to the samples. We obtain each sample with a different step of the phase mask.

2.5 Optical layout of the instrument

The interferometer we designed has a single reference arm and a measurement arm. At the end of the measurement arm, there is a 40 cm silicon mirror. The mirror is suspended and cooled at cryogenic temperatures inside

Downloaded From: https://www.spiedigitallibrary.org/conference-proceedings-of-spie on 20 Dec 2022
Terms of Use: https://www.spiedigitallibrary.org/terms-of-use

the 6.5 m diameter vacuum chamber of the facilities at the Space Center of Liège in Belgium. There is a distance of 3 meters between the silicon mirror and the vacuum chamber optical window. The length of the measurement arm is defined by the architecture to cool down the mirror inside the vacuum chamber.[18] According to the length of the measurement arm, the reference arm is, in principle, 3 m. In Fig. 4 we schematically illustrate the interferometer with the optical layout of a Michelson Interferometer. In this scheme, we have a reference arm that contains the phase mask, a measurement arm with the suspended silicon mirror and we have a low coherence source before the beamsplitter. The aim is that the information from all the local points of the mirror passes through all the steps. We obtain, as a result, an interferogram for each step of the same mirror area. As explained in the previous sections, each step introduces a different OPD.

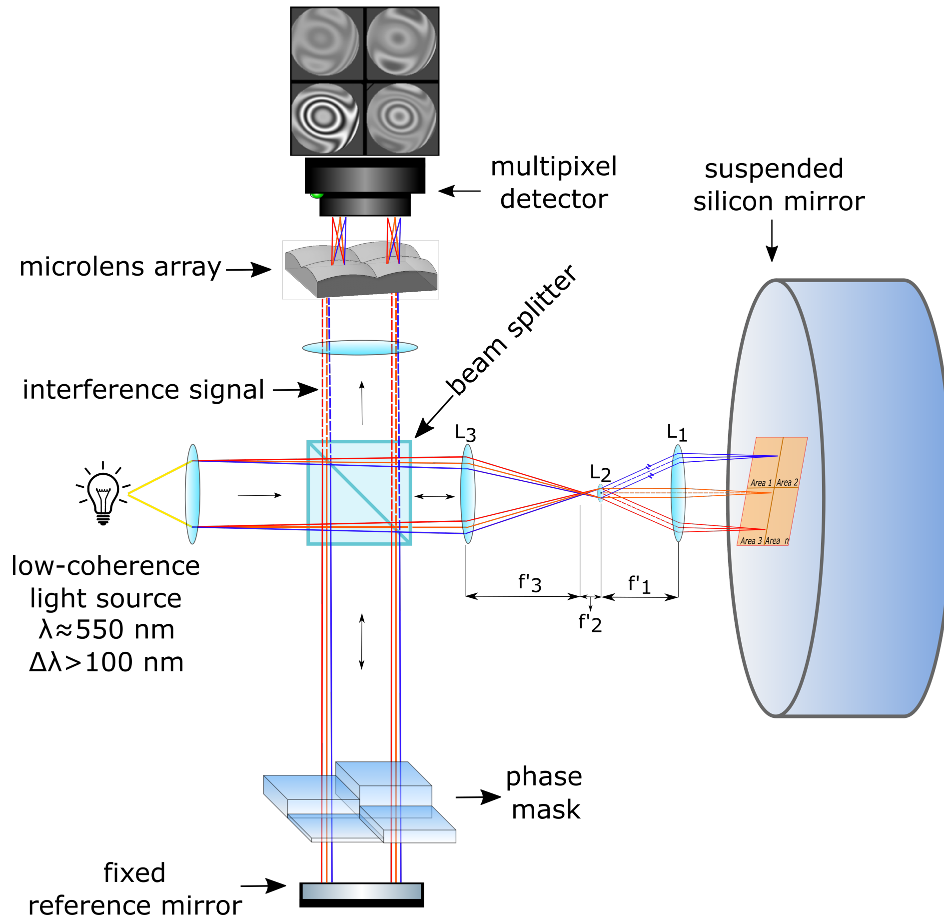

Figure 4. Conceptual view of the metrology instrument we develop to measure the topology change and local vibration of the suspended silicon mirror. The aim is that the information from all the local points of the mirror passes through each phase mask step. As a result, we obtain on a single camera frame a set of interferograms of the same mirror area at different OPDs.

With this aim, we implement an arrangement of lenses on the measurement arm to convert the spatial information onto angular information and to ensure that all the angles pass through all the steps of the phase mask. Besides, we add a microlens array before the detector to image the information from each step of the phase mask. The number of lenses on the microlens array is equivalent to the number of phase mask steps. The lenses on the measurement arm represent a telecentric arrangement with three main lenses. First rays almost parallel from the mirror reach the lens L1. At the focal point of L1, we locate the lens L2. L2 creates an intermediate image of the area observed. The focal point of L2 will be also the focal point of L3, to ensure the afocal arrangement of the lens. At this point, all the angles imaged cover almost all the aperture of the lens L3. Then those rays will pass through the phase mask and cover all the steps. Finally, the microlens array focuses

Downloaded From: https://www.spiedigitallibrary.org/conference-proceedings-of-spie on 20 Dec 2022
Terms of Use: https://www.spiedigitallibrary.org/terms-of-use

on the detector the interferogram associated with each step.

Here we illustrate the interferometer concept through a Michelson Interferometer optical layout for a better understanding. The final optical layout contains a different arrangement of the reference arm and position of the phase mask. The measurement principle and lens arrangement on the measurement arm remain the same.

3. RESULTS

3.1 Computer simulations

The interferogram associated with each step of the phase mask contains the information of the deformation and local vibration of multiple points inside the area observed on the mirror. Fig. 5 a) illustrates the concept of the metrology instrument through a simulation of the interferometer in the optical software ASAP NextGen. This figure represents the four interferograms of the example of mirror deformation of Fig. 5 b) obtained with a phase mask of four steps. We highlight how the entire area observed on the mirror is imaged at each step. For this simulation, we used a spectrum from 400 nm to 600 nm and a central wavelength at 550 nm. Then in Fig. 5 c) we illustrate the reconstruction of the white light interferogram for one of the points inside the area observed. The instrument's lateral resolution will be in the order of a few micrometres, according to the pixel size of the detector.

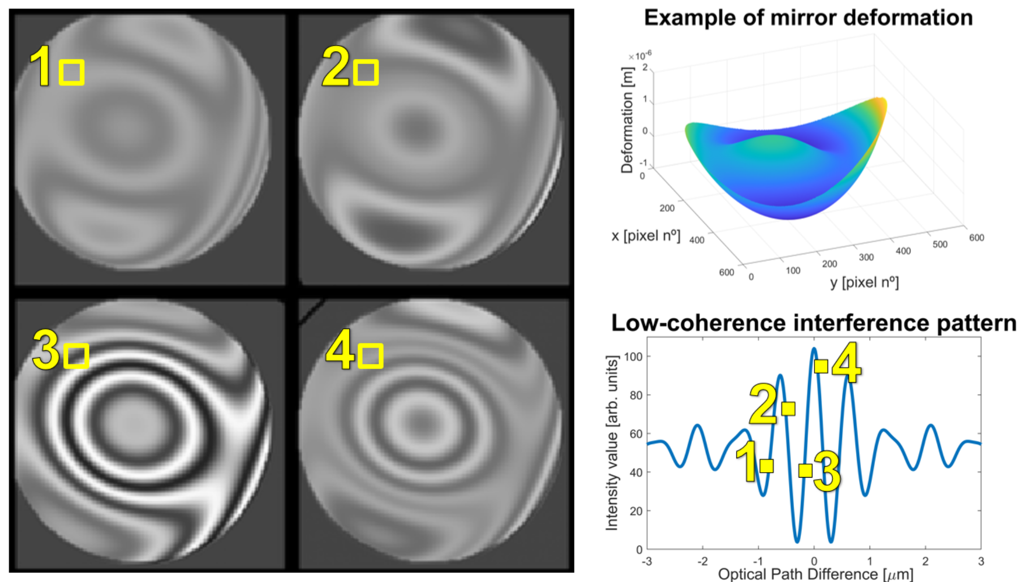

Figure 5. a) ASAP NextGen optical simulation of the interferograms obtained with a phase mask of four steps of the example of mirror deformation (b). c) Reconstruction of the interference pattern for one point. White light source: $\Delta\lambda = 400$ nm to 600 nm; $\lambda_c = 550$ nm.

3.2 Proof of concept of the interferometer

We have started building a proof of concept of the interferometer in the laboratory. Our aim is to replicate the simulation results of Fig. 5 with a scaled version of the instrument. We base the proof of concept at the laboratory on the optical layout of a Michelson Interferometer. On one of the interferometer arms we locate a glass plate of a few millimetres thickness installed over a support that rotates with micrometre precision. The lenses of the measurement arm of Fig. 4 are not included since we need them only for a multiple-step phase mask.

The alignment of a Michelson Interferometer with a white light source is an arduous task. This is due to the small coherence region of a white light source with large bandwidth. We use a tungsten halogen light source

Downloaded From: https://www.spiedigitallibrary.org/conference-proceedings-of-spie on 20 Dec 2022
Terms of Use: https://www.spiedigitallibrary.org/terms-of-use

from Ocean Insight. The lamp model is HL-2000-FHSA-LL. It has a bandwidth at its FWHM of around 400 nm on the visible spectral range between 400 nm to 800 nm, with a peak wavelength of around 600 nm. According to Eq. 2 this correspond to a coherence length of 0.6 μm.

To find the coherence region of the white light source and, therefore, the interference fringes, we first co-align the interferometer with a laser source of large coherence. The laser alignment is represented in Fig. 6 a). Then, we switch to the white light source and modify the length of one of the arms until we find the fringes. Eventually, we also use a bandpass filter in front of the source, of 8 nm at a wavelength of 520 nm. This increases the coherence region while keeping it smaller than the laser. Also, we can install one of the mirrors on a PZT device with nanometer accuracy, as we did in Fig. 6 (4), to find the coherent region. The fringes of equal thickness on a white light interferogram are characterized by a central black fringe and a set of colour fringes whose contrast decreases rapidly with their distance from the central fringe. The black region corresponds to the optical contact. On the other hand, white light Haidinger fringes are characterized by a black circular fringe close to the centre and a set of coloured fringes around with a lower contrast when we move from the centre. The Haidinger fringes or fringes of equal inclination are visible when the measurement mirror and reference mirror reflect the rays with the same angle so that an image is formed at the infinity. If both mirrors were located over the same optical axis, they would need to be parallel to obtain the Haidinger fringes.[12] As a remark, we are using two flat mirrors. The white light interferometer setup is included in Fig. 6 b).

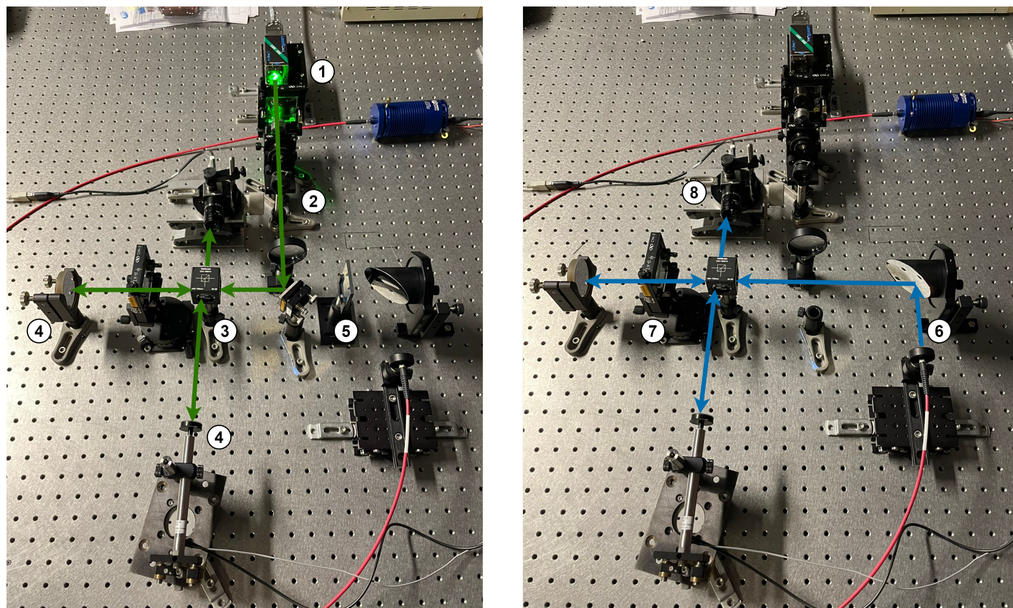

Figure 6. a) Michelson Interferometer using a laser source (1) for alignment purposes. (2) Spatial filtering and collimation of the source, (3) beamsplitter 50/50, (4) flat mirrors and (5) filter to limit the white light source bandpass. b) White light interferometer coaligned with the laser source. (6) Ocean Insight HL-2000-FHSA-LL source thought a fiber and parabolic mirror for collimation, (7) glass plate over a rotating support, (8) Thorlabs CMOS DCC3240M camera.

We align with the glass plate already on one of the arms. Next, we rotate the glass plate and observe the displacement of the fringes. We capture the images with a Thorlabs High-Sensitivity CMOS DCC3240M camera of 1280 x 1024 pixels. In Fig. 7 (1) and (2), we represent two rotations of the glass plate close to the optical contact. From (1) to (2) the central circular fringe is smaller since we get further from the optical contact. We can also notice a lateral displacement of the fringes introduced by the glass plate. We expect not to have this problem with the multistep phase mask. The manufacturers will treat both sides of the phase mask before engraving the steps so they are as planar as possible. The deviation from a circular shape of the fringes is the result of a non perfectly planar mirror and also due to instabilities of the light source. In Fig. 7 (3) and (4), there are two other orientations of the glass plate, this time when the reference mirror is slightly tilted for better

Downloaded From: https://www.spiedigitallibrary.org/conference-proceedings-of-spie on 20 Dec 2022
Terms of Use: https://www.spiedigitallibrary.org/terms-of-use

visualization. We see how from (3) to (4) the space between fringes increases since we approach the circular fringes. Also, we can again appreciate the lateral displacement of the fringes to one side of the interferogram.

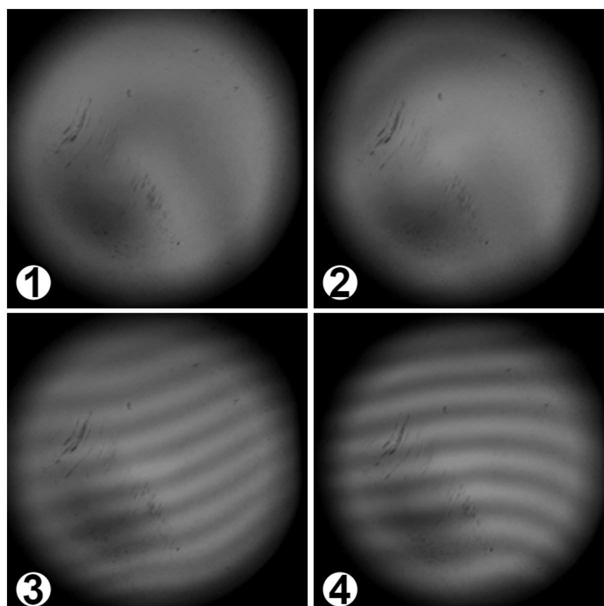

Figure 7. Four interferograms obtained with a low-coherence white light source and captured with a CMOS camera. (1) and (2) are the Haidinger fringes close to the optical contact. From (1) to (2) we rotate the glass plate on one of the interferometer arms to simulate two steps of the phase mask. Same procedure on (3) and (4) but this time with linear fringes for better visualization. We can appreciate the displacement of the fringes due to the phase shift introduced by a different optical thickness of the glass plate.

On the other hand, we can vary the length of one of the arms and observe the quick contrast change of the fringes. The fringes are only visible in a region smaller than 1 μm according to the coherence length of our source. In Fig. 8 there are represented four interferograms corresponding each one to the same mirror inclination and different consecutive lengths of one of the interferometer arms. This is according to the results simulated in Fig. 5

4. DISCUSSION

One of the first conclusions from the proof of concept is that we can obtain the fringes of interference even with a very large bandwidth on the visible and therefore very low coherence. We used a source of 400 nm FWHM bandwidth on the visible from 400 nm to 800 nm. This does not mean that having such a large bandwidth is better than just half or even less. The sampling needed by the processing algorithm of the white light interferograms will determine the best coherence length to detect the position of the mirror with the accuracy desired. The bandwidth is therefore related to the number of steps of the phase mask. Another positive result is to observe the displacement of the fringes with different thicknesses of a glass plate which proves the working principle of the phase mask.

On the proof of concept, we observed that we need to improve the fringe contrast for better visualization of the fringes. We can introduce neutral density filters or use beamsplitters different than 50 R and 50 T. We confirmed the strong effect of vibrations on the visibility of the fringes. Therefore, it is clear that the capability of our instrument to instantaneously capture full interferogram maps on a single camera frame will be a large advantage.

Another point studied with the proof of concept is the maximum length of the interferometer arms. This is important since the distance between the suspended silicon mirror under study and the first optical element of

Downloaded From: https://www.spiedigitallibrary.org/conference-proceedings-of-spie on 20 Dec 2022
Terms of Use: https://www.spiedigitallibrary.org/terms-of-use

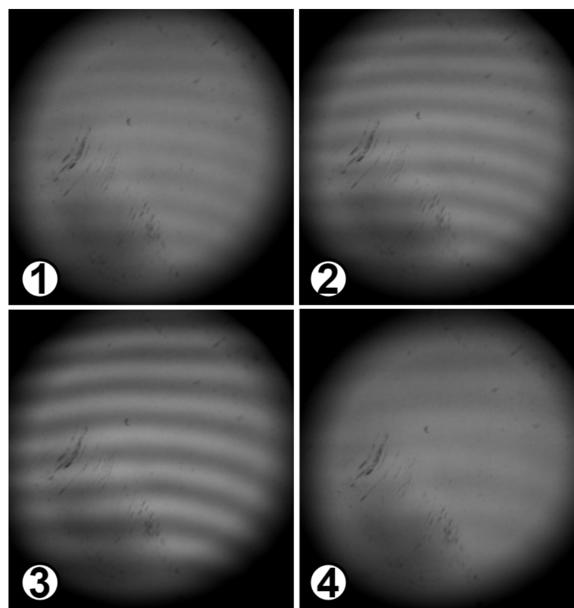

Figure 8. Four interferograms obtained with a low-coherence white light source and captured with a monochromatic camera. From (1) to (4), we increase the length of one of the interferometer arms, while we keep the inclination of the mirror constant. On (3) is where the contrast is higher which represents the point where the lengths of the two arms of the interferometer are more equalized. The range where the fringes are visible is less than 1 μm.

the metrology instrument is at least 3 m. The main limiting factor at the moment to reach the 3 meters is the low power of the source. We study the need for a more powerful source or a supercontinuum white-light laser.

5. CONCLUSION

We presented an update on the state of the development of the metrology instrument. We explained the measurement principle of the device. It can obtain a set of interferogram maps of the mirror at different OPDs and on a single camera frame. With this instrument, we can measure local vibration and topology change of the suspended silicon mirror.

In addition, we presented the first experimental results of a proof of concept of the metrology instrument to prove some of its capabilities. First, we can obtain the interference fringes with a source of very low coherence. We used a source of FWHM bandwidth of 400 nm in the visible between 400 nm to 800 nm. Then, we showed how we could modify the OPD with a glass plate of different thicknesses like on the phase mask. With the proof of concept, we detected some of the significant challenges of the instrument. These are, first, the complexity of the alignment of a white light interferometer with large arms because of the intensity lost and the small region of coherence. And second, the problem we had with the fringe contrast due to intensity inequalities between the arms of the interferometer.

The next step is to perform a tolerance study of the phase mask and manufacture it. The mirror characterization of GW detectors on operation is essential to ensure the accuracy of the detection of the gravitational waves.

ACKNOWLEDGMENTS

The E-TEST project is carried out within the framework of the Interreg V-A Euregio Meuse-Rhine Programme, with 7,5 million euros from the European Regional Development Fund (ERDF). By investing EU funds in Interreg projects, the European Union is investing directly in economic development, innovation, territorial development, social inclusion and education in the Euregio Meuse-Rhine .

Downloaded From: https://www.spiedigitallibrary.org/conference-proceedings-of-spie on 20 Dec 2022
Terms of Use: https://www.spiedigitallibrary.org/terms-of-use

REFERENCES

[1] Einstein Telescope Science Team, "Einstein gravitational wave Telescope Conceptual Design Study," tech. rep. (2011).

[2] Kaneda, H., Nakagawa, T., Enya, K., and Onaka, T., "Cryogenic optical testing of SIC mirrors for ASTRO-F and C/SIC composite mirrors for SPICA," *European Space Agency, (Special Publication) ESA SP* (554), 699–706 (2004).

[3] Vilaboa Pérez, J. and Loicq, J., "Dynamic short- and large-coherence interferometry to characterize the induced vibrations and topology change of the cryogenic mirror of the Einstein Telescope prototype," *Optics and Photonics for Advanced Dimensional Metrology II* **121370T**(Proc. SPIE 12137) (2022).

[4] Sandoz, P., Devillers, R., and Plata, A., "Unambiguous profilometry by fringe-order identification in white-light phase-shifting interferometry," *Journal of Modern Optics* **44**, 519–534 (1997).

[5] De Groot, P. and Deck, L., "Surface profiling by analysis of white-light interferograms in the spatial frequency domain," *Journal of Modern Optics* **42**(2) (1995).

[6] Deng, Y. and Chu, D., "Coherence properties of different light sources and their effect on the image sharpness and speckle of holographic displays," *Scientific Reports* **7**, 1–12 (2017).

[7] Millerd, J. E. and North-Morris, M., "Dynamic interferometry: measurement of space optics and structures," *Optical Measurement Systems for Industrial Inspection X* **10329G** (2017).

[8] Ferrec, Y., Bonnery, G., Brooker, L., Croizé, L., Gousset, S., and Le Coarer, E., "Nanocarb part 1: compact snapshot imaging interferometer for co2 monitoring from space," *International Conference on Space Optics - ICSO 2018* **11180** (2019).

[9] Pavliček, P. and Mikeska, E., "White-light interferometer without mechanical scanning," *Optics and Lasers in Engineering* **124** (2020).

[10] Groot, P. D., "Principles of interference microscopy for the measurement of surface topography," *Advances in Optics and Photonics* **7**, 1–65 (2015).

[11] Woo Jeon, J., Won Jeong, H., Bin Jeong, H., and Joo, K., "High-speed polarized low coherence scanning interferometry based on spatial phase shifting," *Applied Optics* **58**(20), 5360–5365 (2019).

[12] Malacara, D., [*Optical Shop Testing*], Wiley-Interscience, 3 ed. (2006).

[13] Kim, J. H., "High precision signal processing algorithm for white light interferometry," *Sensors* **8**(12), 7609–7635 (2008).

[14] Lehmann, P., "Aspect ratio of elongated polychromatic far-field speckles of continuous and discrete spectral distribution with respect to surface roughness characterization," *Applied Optics* **41**, 10–12 (2002).

[15] Lehmann, P., Kühnhold, P., and Xie, W., "Reduction of chromatic aberration influences in vertical scanning white-light interferometry," *Measurement Science and Technology* **25**(6) (2014).

[16] Wiersma, J. T. and Wyant, J. C., "Vibration insensitive extended range interference microscopy," *Applied Optics* **52**, 5957–5961 (2013).

[17] Goodwin, E. P. and Wyant, J. C., [*Field Guide to Interferometric Optical Testing*], SPIE Press, 1 ed. (2006).

[18] Di Pace, S., Mangano, V., Pierini, L., Rezaei, A., Hennig, J.-S., Hennig, M., Pascucci, D., Allocca, A., Tosta e Melo, I., Nair, V. G., Orban, P., Sider, A., Shani-Kadmiel, S., and van Heijningen, J., "Research facilities for Europe's next generation gravitational-wave detector Einstein Telescope," *Galaxies* **10**(3) (2022).

Downloaded From: https://www.spiedigitallibrary.org/conference-proceedings-of-spie on 20 Dec 2022
Terms of Use: https://www.spiedigitallibrary.org/terms-of-use